# Nanoscale Spatial Distribution of Tethered DNA on Model Nucleic Acid Sensor Surfaces

By: Eric A. Josephs and Tao Ye

Josephs, E. A. and T. Ye. "Nanoscale Spatial Distribution of Tethered DNA on Model Nucleic Acid Sensor Surfaces." *ACS Nano,* **2013***, 7* (4)*,* 3653–3660.
http://dx.doi.org/10.1021/nn400659m



## Abstract:

The nanoscale arrangement of the DNA probe molecules on sensor surfaces has a profound impact on molecular recognition and signaling reactions on DNA biosensors and microarrays. Using electrochemical atomic force microscopy, we have directly determined the nanoscale spatial distribution of thiolated DNA that are attached to gold *via* different methods. We discovered significant heterogeneity in the probe density and limited stability for DNA monolayers prepared by the backfilling method, that is, first exposing the surface to thiolated DNA then "backfilling" with a passivating alkanethiol. On the other hand, the monolayers prepared by "inserting" thiolated DNA into a preformed alkanethiol monolayer lead to a more uniformly distributed layer of DNA. With high-resolution images of single DNA molecules on the surface, we have introduced spatial statistics to characterize the nanoscale arrangement of DNA probes. The randomness of the spatial distribution has been characterized. By determining the local densities surrounding individual molecules, we observed subpopulations of probes with dramatically different levels of "probe crowding". We anticipate that the novel application of spatial statistics to DNA monolayers can enable a framework to understand heterogeneity in probe spatial distributions, interprobe interactions, and ultimately probe activity on sensor surfaces.

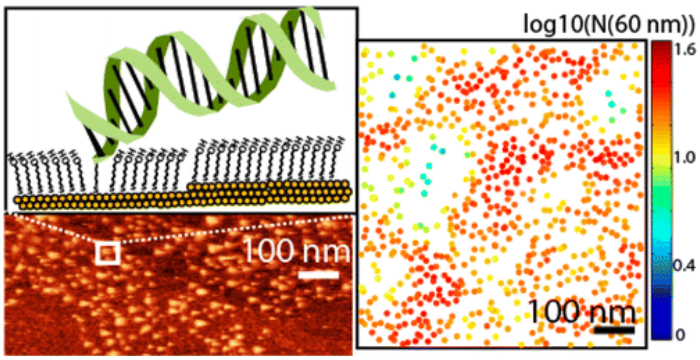


**Keywords:** nucleic acid sensors | alkanethiol self-assembled monolayers | electrochemical atomic force microscopy | second-order spatial analysis | molecular crowding

## Article:

Monolayers of thiolated DNA on gold (Figure 1), which are passivated with inert alkanethiolate monolayers, represent some of the most well-defined surfaces for biosensors.[1-3] These surfaces have been used to detect a wide array of biomarkers, including nucleic acids, small molecules, ions, and proteins.[3] An important challenge in the DNA sensors is understanding and controlling the conformations, orientation, and spatial distribution of the immobilized DNA probes, which impact the sensitivity, selectivity, and reproducibility of these sensors. For example, compared to those in bulk solution, the hybridization rate and binding affinity are notably lower on surfaces,[4-8] due to the electrostatic and steric repulsions that reduce accessibility of the target molecules to the surface probes (the crowding effect). However, despite intense efforts in DNA sensors and microarrays, a molecular-scale picture of the nanometer-scale structures and interactions of the monolayer surfaces has yet to emerge. Existing studies rely on ensemble measurements that are averaged over at least micrometer scale on surfaces using techniques such as fluorescence,[7] surface plasmon resonance,[4] second harmonic generation,[9] quartz crystal microbalance,[10] and electrochemical methods.[11] As the interprobe interactions are highly sensitive to the nanoscale separations between the probe molecules,[5] average densities, which do not account for local variations in interprobe spacing or molecular clustering, are only crude indicators of such interactions. In addition, these techniques often provide limited information concerning the interaction between the DNA probes and the passivating monolayer, which may be heterogeneous at the nanoscale.[12, 13]

Our knowledge in this area would be significantly advanced if the lateral positions of the individual probe molecules could be determined with nanometer precision. Currently, atomic force microscopy (AFM)[19] is the only technique that potentially has the resolution to meet the challenge. However, the DNA molecules on biosensor surfaces are too mobile to resolve clearly because the surfaces are typically passivated with inert functional groups to inhibit nonspecific adsorption of nucleic acids.[1] Recently, we demonstrated that, by applying positive electrode potentials, AFM could resolve individual DNA molecules tethered to a SAM-passivated surface under a buffer solution.[12, 13] While we previously focused on the electric-field-dependent conformations and surface interactions of *single* DNA molecules,[12, 13] here we sought to directly investigate—at the molecular scale— how *the spatial distribution* of DNA molecules across the surface was influenced by the probe design and surface coupling method. Our real-space, nanoscale measurements show that the thiolated DNA monolayers prepared by the popular backfilling method (Figure 1C) may not be optimal due to the tendency for probe molecules to cluster and the limited stability of the passivating SAM. By contrast, the insertion method, which attaches DNA to a preformed SAM (Figure 1B), yields more uniform distribution of the DNA. We have applied spatial statistics to characterize the distributions of DNA molecules: we find that the spatial distribution of DNA molecules that are attached *via* the insertion method is neither uniform nor completely random. Moreover, we can determine the local densities of DNA molecules around each molecule over the distances at which the molecules are likely to interact. Subpopulations with dramatically varying levels of "probe crowding" have been observed on the surface. These spatial statistics, which have not appeared in the biosensing literature to the best of our knowledge, may provide a more natural framework for elucidating the molecular-scale mechanisms of sensor performance, such as density-dependent effects of molecular recognition.

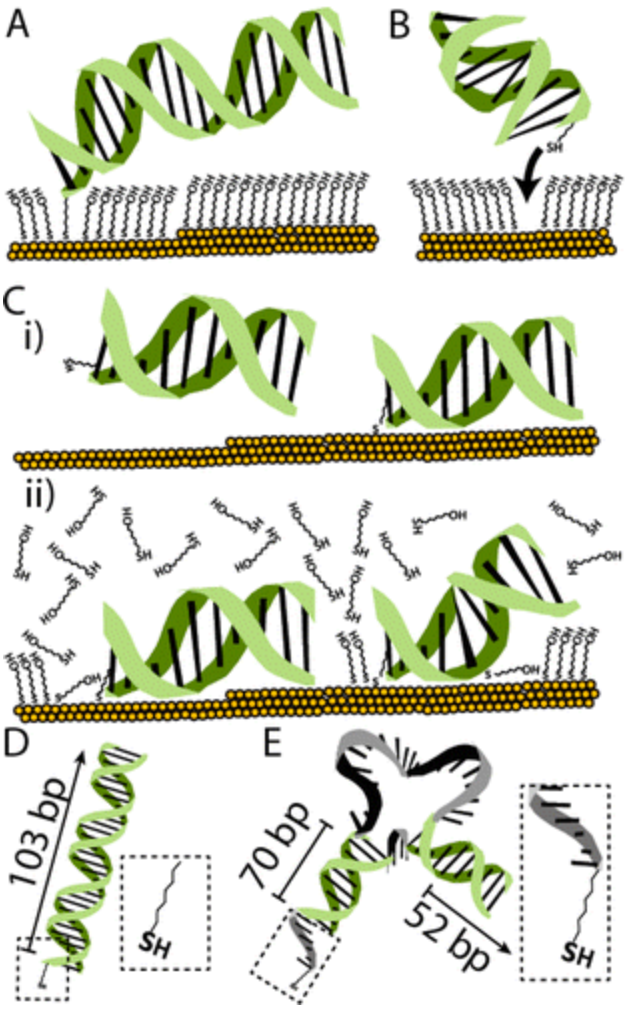


**Figure 1.** (A) Schematic of the structure of a model nucleic acid sensor surface: DNA probes are tethered by a hexanethiol linker (C6SH) to a gold electrode surface, which has been passivated by a 6-mercaptohexanol (MCH) monolayer. (B) "Insertion" method of assembly. A gold surface first passivated by MCH is exposed to thiolated DNA, which preferentially attaches to the surface at defect sites in the monolayer. (C) "Backfilling" method of sensor surface assembly. (i) Gold surface is first exposed to thiolated DNA and (ii) then immersed in a solution of MCH, which lifts the DNA off the surface. (D,E) Schematic of DNA structures assembled on the surface for this study (not to scale). (D) Double-stranded DNA (the C6SH ds) anchored to the surface by the C6SH linker (inset). (E) T5C6SH ss/ds with both single-stranded (gray) and double-stranded (green) DNA segments (see text). Five unpaired thymine bases are incorporated between the C6SH linker and a double-stranded segment (T5C6SH, inset) to help separate the active region of the probes from the MCH SAM, a commonly used strategy to facilitate target binding or signaling reactions.[14-18]

**Results and Discussion**

The DNA molecules are anchored *via* a Au–S bond between the gold surface and the 5′-hexanethiol tethers (C6SH), whose length matches that of 6-mercaptohexanol (MCH), which is commonly used to passivate the gold surface (Figure 1A).[1] Two different DNA designs are used

in this study (Figure 1D,E). In the C6SH dsDNA (Figure 1D), a C6SH tether is directly attached to the 105 bp dsDNA.[12] Surface-anchored dsDNA, which can be denatured under mild conditions, are precursors to single-stranded probes in some studies;[4] hence, their locations on the surface can serve as a proxy for single-stranded probes which are more difficult to resolve with AFM. Moreover, dsDNA probes have also been directly used in biosensors based on electric-field-induced orientational switching.[20-22] On the other hand, a number of novel signal transduction mechanisms rely on DNA probes that have both single-stranded and double-stranded segments.[3, 6, 23-25] To understand how such probe designs influence SAM stability as well as the spatial distribution and orientation of the probes,[26] we have also used a T5C6SH ss/dsDNA (Figure 1E). This structure is an analogue of a catalytic beacon probe[14, 25] that possesses a single-stranded DNAzyme domain[27] capable of catalyzing the cleavage of ribonucleotides. The design used here is inactive due to the lack of ribonucleotides.[27, 28]

The method of backfilling with alkanethiols (Figure 1C) remains the most prevalent method to prepare the thiolated DNA sensor surface.[1, 2, 4, 5, 14, 21] Although it was initially assumed that the DNA molecules are uniformly distributed in the monolayers,[1, 4, 11] a number of ensemble studies suggest that the surface may in fact be heterogeneous in probe orientation and surface density.[21,29] Using fluorescence microscopy to image DNA monolayers on gold with micrometer resolution, Bizzotto *et al.* discovered direct evidence of significant heterogeneity in probe densities.[30]

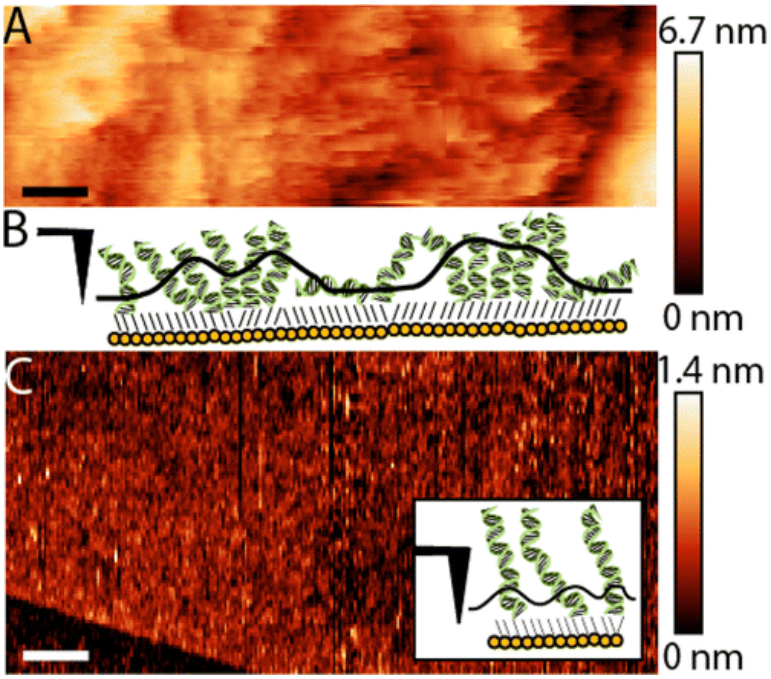


**Figure 2.** (A) Tapping mode AFM of a high probe density surface prepared by backfilling C6SH dsDNA with MCH (after 1 h exposure to a 5 nM probe solution). Topographical imaging reveals heterogeneity in probe density on the scale of tens of nanometers. (B) Schematic showing that clustering of DNA results in apparent differences of topographical heights. (C) Surface with lower DNA density prepared by backfilling C6SH dsDNA with MCH (after 5 min exposure to a solution that contains 5 nM DNA). Scale bars are 100 nm.

To understand the heterogeneity at the molecular scale, we performed tapping mode AFM of a DNA monolayer surface that was prepared by exposing a gold surface first to a 5 nM solution of C6SH probes for 1 h and then to an aqueous solution of MCH (Figure 2A). Although the average density of DNA on the (111) facet was not quantified with standard electrochemical techniques[11] due to the existence of different facets on our gold bead substrate, the surface concentration of this surface is estimated to be between $10^{12}$ and $10^{14}$/cm$^2$ based on the estimates of bulk surface concentrations from surfaces where we could directly resolve individual molecules (*i.e.*, Figure 3 and Figure 4; see Table 1). The features observed, with apparent heights of several nanometers, cannot be individual DNA molecules that adopt an upright orientation, as such molecules would be too mobile to resolve by AFM.[12] Rather, as previously observed in exclusively DNA monolayers containing no additional alkanethiols[31, 32] as well as in nanopatterned thiolated DNA,[33, 34] these features correspond to aggregated clusters where the tightly packed DNA molecules are forced off the surface (Figure 2B).[35] The surface is in marked contrast with pure DNA monolayers, which display much lower roughness (<1 nm).[31,32] Therefore, the backfilling of MCH is responsible for the aggregated DNA structures observed in Figure 2A: due to the labile nature of the thiol–gold bond at low surface coverages,[12, 36] upon the addition of MCH, the thiolated DNA molecules likely diffuse laterally to form aggregates that are energetically favored.

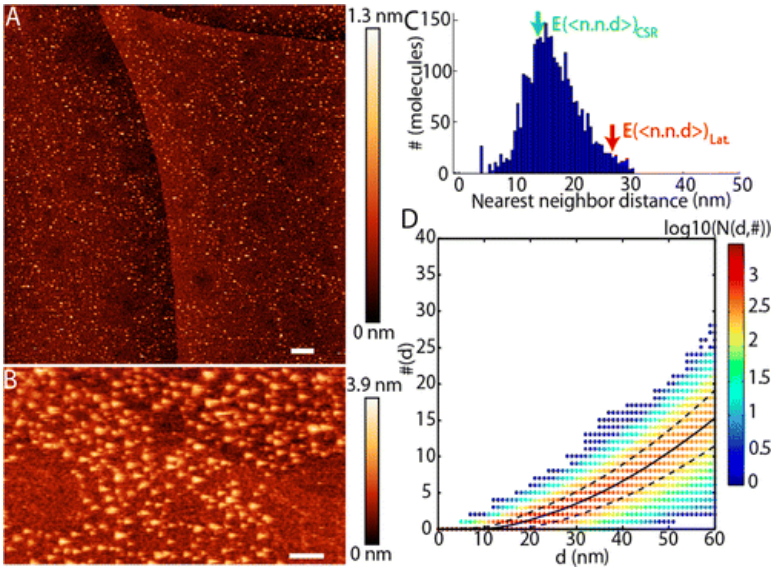


**Figure 3.** (A) Tapping mode image of T5C6SH ss/dsDNA probes in MCH under sodium acetate-supplemented (25 mM) 1× TAE buffer (at +600 mV) prepared by the insertion method. Note the large circular regions with no protrusions. (B) Close-up image of T5C6SH DNA surface at open circuit potential. (C) Histogram of distances from each DNA molecule to its nearest-neighboring DNA molecule (n.n.d.) from panel A. Green and red arrows indicate expected mean n.n.d. of either complete spatial randomness ($E(\langle\text{n.n.d.}\rangle)_{CSR}$) or a perfectly ordered lattice spatial distribution ($E(\langle\text{n.n.d.}\rangle)_{Lat.}$) of a surface with the same average density. (D) Histogram of the "crowding distribution function" $N(d,\#)$, the number of DNA molecules with # other DNA molecules within a distance $d$ (see text). Line with dots is the mean #($d$) ($\langle\#(d)\rangle$), dashed lines indicate $\langle\#(d)\rangle \pm$ standard deviation if >0.

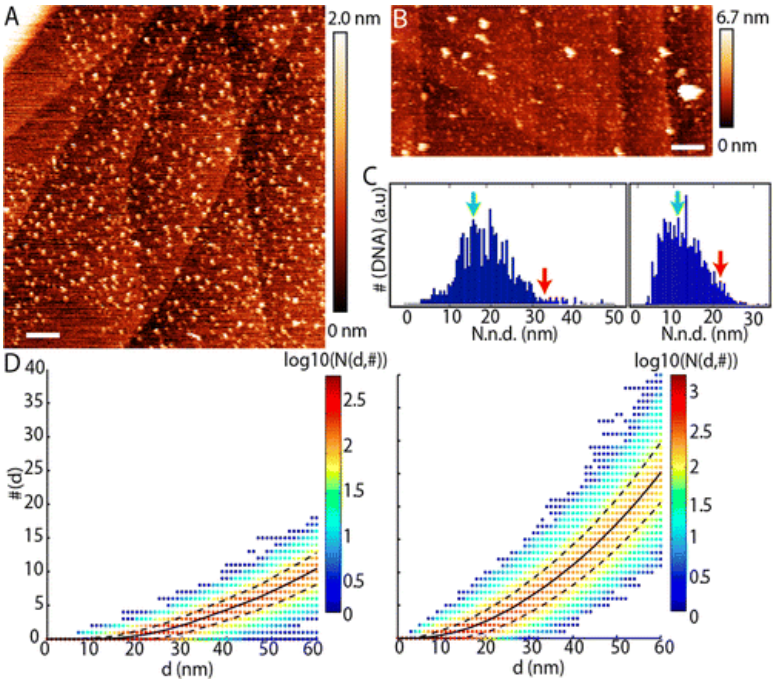


**Figure 4.** (A) Tapping mode AFM image of a thiolated DNA monolayer prepared by the insertion method, *i.e.*, exposing an MCH SAM to a 5 nM solution of C6SH probes. The image was acquired at open circuit potential. Note the large circular regions with low DNA density in panel A, which are similar to those found in Figure 3A. (B) Surface prepared by the insertion method using an increased concentration of C6SH, 500 nM. Some taller aggregated features are observed. Scale bars are 100 nm. (C) Normalized histograms of n.n.d. (aggregated features in panel B were excluded from analysis). Green and red arrows indicate $E(\langle \text{n.n.d.} \rangle)_{\text{CSR}}$ or $E(\langle \text{n.n.d.} \rangle)_{\text{Lat.}}$, respectively (see Figure 3). (D) Histograms of the crowding distribution function $N(d,\#)$ (see text) for (left) panel A and (right) panel B, respectively.

**Table 1.** Experimentally Measured and Expected Nearest-Neighbor Distances (n.n.d.) from Estimated Bulk Densities of Thiolated DNA

| | **estimated average surface density/(molecules/cm$^2$)** | **$\langle$n.n.d.$\rangle$ ± SD** | **$(A/n)^{1/2} = E(\langle \text{n.n.d.} \rangle)_{\text{Lat.}}$** | **$E(\langle \text{n.n.d.} \rangle)_{\text{CSR}}$** |
|---|---|---|---|---|
| Figure 3A($n$ = 3003) | $1.3 \times 10^{11}$ | 17.1 ± 5.3 nm | 27.4 nm | 13.8 nm |
| Figure 4A($n$ = 951) | $9.5 \times 10^{10}$ | 22.1 ± 6.5 nm | 32.4 nm | 16.4 nm |
| Figure 4B($n$ = 1909, nonaggregated features) | $>2.2 \times 10^{11}$ | 12.4 ± 4.9 nm | <21.2 nm | <10.7 nm |

On the other hand, surfaces with lower densities of C6SH molecules (prepared *via* a shorter (5 min) exposure prior to backfilling with MCH, Figure 2C and Figure S1 in Supporting Information) appeared significantly more uniform: due to the reduced roughness of the monolayer, even the atomic steps of the gold substrate are clearly resolved. Hence high densities of DNA on the surface promote aggregation during backfilling.

An additional concern for electrochemical DNA sensors is the integrity of the passivating layer under applied potentials. *In situ* AFM provides direct evidence that the passivating MCH monolayer prepared by the backfilling method degrades within minutes at +600 mV *vs* Ag/AgCl (Figures S2–S4). By contrast, pure MCH SAM or those SAMs with significantly lower probe

concentrations (Figure S5) degrade much more slowly. As independent electrochemical methods found that backfilled MCH SAMs, particularly those with higher probe concentrations, are more defective,[37] the desorption of the MCH molecules is likely accelerated by the presence of defects.

On the other hand, after preparation of a T5C6SH ss/dsDNA monolayer *via* the insertion method (Figure 1B), the negatively charged molecules could be pinned to the surface at +600 mV and resolved by AFM individually (Figure 3A), consistent with the results in our previous study.[12] The DNA molecules appeared as small round protrusions, which we previously have attributed to the segment closest to the tether. The segment is relatively stationary due to constraint by the tether and the electric field;[12] the rest of the DNA remains too mobile to resolve clearly. In this case, the MCH monolayer was significantly more stable than backfilled MCH monolayers (Figure S5). Both T5C6SH and C6SH (Figure 4A) on surfaces prepared with the insertion method appeared isolated and evenly distributed on their respective surfaces, except that there were several circular regions tens to hundreds of nanometers in diameter where no DNA could be observed. Such heterogeneity would be difficult to discern using existing ensemble techniques or light microscopy. Previous scanning tunneling microscopy studies of the MCH SAM found that the surface consists of ordered and disordered domains of the thiol molecules.[38] Because the alkanethiols at SAM defect sites are more likely to be exchanged with thiolated DNA in solution,[39, 40] we attribute the regions free of DNA molecules to highly ordered SAM domains that contain far fewer defects. From the large area image in Figure 3A, we estimate that the average surface density of the inserted T5C6SH surface was $1.3 \times 10^{11}/\text{cm}^2$, and the surface prepared by insertion of C6SH in Figure 4A was $9.5 \times 10^{10}/\text{cm}^2$ (Table 1).

If the MCH SAM is exposed to a ~500 nM C6SH dsDNA solution, which is a hundred times as concentrated as before, the surface density increases and the empty circular regions are no longer observed (Figure 4B). The taller features likely correspond to aggregated DNA molecules, though they make up only a small fraction of the surface coverage (approximately 4%). We estimate the average surface density of (nonaggregated) DNA to be $2.2 \times 10^{11}$ molecules/cm$^2$ (Table 1), about twice that in Figure 4A, even though the surface was exposed to DNA solutions that are 100× more concentrated. The sublinear dependence on the concentration of thiolated DNA solution suggests that, at higher DNA concentrations, the insertion process is limited by the number of available defects in the SAM.

While AFM imaging can provide average surface densities of DNA, which can be compared to those obtained with ensemble techniques,[1, 9, 10, 41] we can also extract information that is relevant to molecular recognition and difficult or impossible to obtain with existing techniques. As the nearest-neighbors are expected to have the largest impact on interprobe interactions, the nearest-neighbor distance is likely a determining factor for the activity of a probe molecule. Because only the number of probes ($n$) and total surface area ($A$) of the sample can be measured using common ensemble techniques, the mean nearest-neighbor distance ($\langle$n.n.d.$\rangle$) is often estimated as $(A/n)^{1/2}$.[5, 6, 42, 43] However, this is only the expected mean n.d.d. if the probes are arranged in a square lattice ($E(\langle\text{n.n.d.}\rangle)_{\text{Lat.}}$) and will overestimate the $\langle$n.n.d.$\rangle$ if there is any aggregation or randomness in the spatial distribution. An alternative estimate for $\langle$n.n.d.$\rangle$ assumes that the distribution of probes on the surface exhibits complete spatial randomness (CSR)[44] and is estimated by $E(\langle\text{n.n.d.}\rangle)_{\text{CSR}} = 0.5(A/n)^{1/2} + (0.051 + 0.042/n)(P/n)$, where $A$ is the

area of the imaged region, $n$ is the number of probe molecules in that region, and $P$ is the perimeter of that region. That is, $E(\langle \text{n.n.d.} \rangle)_{CSR} \approx 1/2E(\langle \text{n.n.d.} \rangle)_{Lat.}$. However, this value may underestimate the ⟨n.n.d.⟩ if the distribution is not completely random. In this study, the molecular resolution AFM images enable the direct measurement of the distribution of nearest-neighbor distances (Figures 3C and 4C). For the DNA immobilized using the insertion method, the $E(\langle \text{n.n.d.} \rangle)_{CSR}$ is closer to the experimental means (Table 1), regardless of density or DNA design, while $E(\langle \text{n.n.d.} \rangle)_{Lat.}$ overestimates the experimental ⟨n.n.d.⟩ by nearly 100%. That $E(\langle \text{n.n.d.} \rangle)_{CSR}$ is slightly smaller than the experiment value implies that the distribution of probes is not completely random (see below).

Other higher-order spatial statistics can provide a measure of the molecular-scale distribution and clustering of DNA molecules beyond the distance of the nearest-neighbors. A 2D autocorrelation function (ACF) can provide some information concerning nanoscale probe crowding (Figure S6)—indeed, a radial minimum is observed in each ACF slightly closer than the respective mean n.n.d., indicative of the lack of probes around each molecule at that radius. However, the 2D ACFs can obscure how the density of probes locally varies in the absence of longer-range correlations. To characterize the local variation of the probe density, we define a crowding function $N_i(d)$ as the edge-weighted number of others molecules within a radius $d$ of the molecule of interest, i: $N_i(d) = \Sigma_{j \neq i} w_{ij}^{-1} I_{(d-dij)}$, where $d_{ij}$ is the distance between molecules $i$ and $j$, $w_{ij}$ is a factor which compensates for DNA molecules near the edge of the image (see Supporting Information),[45] and $I_{(d-dij)}$ is an indicator function (equals 1 if $d - d_{ij} \geq 0$ and 0 otherwise). The crowding distribution $N(d,\#)$ is the total number of DNA molecules that have # other DNA molecules within a distance, $d$. $\langle \#(d) \rangle / (n/A)$, the density-normalized mean number of other DNA molecules around each DNA molecule, is also known as Ripley's $K$ function $K(d)$,[46] which is commonly used in spatial statistics because of its ability to preserve both long- and short-range information in tests of complete spatial randomness ($K(d) \approx \pi d^2$ for CSR processes).

Graphs of $N(d,\#)$ can be used to directly visualize the local densities surrounding each DNA molecule and how crowding varies across the surface. Figure 3D and Figure 4D show the two-dimensional histograms for $N(d,\#)$ for each DNA from Figure 3A and Figure 4A,B with $d = 0$ to 60 nm (approximately twice the contour length of the C6SH dsDNA). In all cases, the DNA rarely have a neighboring molecule within 10 nm, and the vast majority have less than two other molecules within 20 nm, except for those in the aggregated features in Figure 4B. Additionally, each molecule within the same image tends to be surrounded by a similar number of other molecules. The standard deviations in the distribution of the number of other DNA molecules within 60 nm are all less than 5 molecules. For comparison, hypothetical surfaces with completely randomly distributed DNA molecules have larger standard deviations (Figure S7).[44] Both the narrow distributions of the crowding functions and the fact that the experimental nearest-neighbor distances are larger than $E(\langle \text{n.n.d.} \rangle)_{CSR}$ imply some level of molecular-scale ordering. This ordering may be a result of the "insertion" method used to immobilize the DNA molecules, where DNA are preferentially incorporated into SAM defects that cannot accommodate multiple DNA molecules in the same site. Although the Debye length of the DNA solution is only 1.1 nm, we cannot yet completely rule out the possibility that electrostatic repulsion affects the spatial distribution of inserted molecules, as a DNA molecule anchored to the surface may rotate and reduce the probability of incorporation of a DNA in its proximity.

Additional studies are underway to understand how the electrostatic repulsion between DNA molecules may be exploited to optimize the nanoscale spatial distribution.

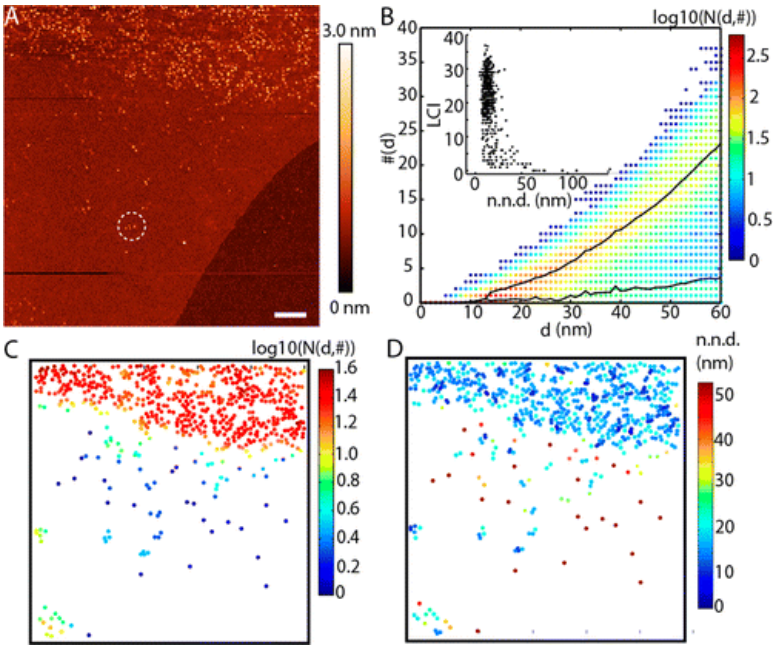


**Figure 5.** (A) Tapping mode AFM image of T5C6SH inserted into MCH SAM where two populations (high density and low density) are apparent. The dashed white circle highlights a low density region of probes with nearest-neighbor distances similar to those in the high density regions. (B) Histogram of the crowding distribution function $N(d,\#)$ for the surface in panel A. Lines with dots are the means from fitting the $N(d,\#)$ at each $d$ as the mixture of two Gaussian distributions. (Inset) Plot of $N(60\text{ nm})$ *vs* n.n.d. for each DNA molecule shows that DNA molecules in both the high-density and low-density regions may have similar nearest-neighbor distances despite large differences in local density. (C) Local crowding index, defined here as $N(60\text{ nm})$ (see main text) and (D) nearest-neighbor distance graphed at the respective locations of the probes from panel A.

In addition to histograms, we displayed the local crowding index, LCI, at the location of each of the molecules. LCI is the number of DNA molecules that can potentially interact with a particular DNA molecule (defined here by $N(60\text{ nm})$ for the molecule of interest; 60 nm is twice the length of the thiolated DNA). Subpopulations of DNA molecules with lower LCIs can be identified within the mostly empty circular regions from Figure 3A and Figure 4A (Figures S8 and S9). Figure 3A also possesses bands of DNA molecules with alternating higher and lower LCIs around the circular regions. The image in Figure 5A is of a surface with a T5C6SH DNA/MCH SAM that exhibits distinct DNA densities in larger areas. The heterogeneity in DNA density observed is likely related to the micrometer-scale fluorescence intensity variations observed on labeled DNA monolayers in the study by Bizzoto and co-workers.[30] In this case, the heterogeneity leads to a distinctly bimodal $N(d,\#)$, and the resulting crowding distribution can be fit as the mixture of two Gaussian distributions (Figure 5B). The LCI map (Figure 5C) shows that the LCIs are uniform within those respective regions; the LCIs in the high-density region are similar to those of Figure 3A (Figure S8), and a distinct interfacial region between the two can also be discerned. The n.n.d. map on the other hand does not discriminate as well between

subpopulations of DNA molecules in the high-density and low-density regions (Figure 5D). Therefore, the LCIs are a more natural descriptor to quantify DNA density on sensor surfaces and test molecular-scale mechanisms of sensor assembly and performance. In fact, many molecules within the low-density regions of Figure 5A have nearest-neighbor distances similar to those within the high-density regions (Figure 5B inset). Future *in situ* studies that can follow the insertion process will be needed to test the possibility that insertion events into the SAM may not be as random as commonly assumed: DNA incorporation into larger defects may, in turn, disrupt the local SAM and create more opportunities for other DNA molecules to attach nearby.

## Conclusions

Our study clarifies a number of outstanding questions concerning the spatial distribution of the DNA molecules and the stability of the passivating SAM in thiolated DNA monolayers. The results provide direct evidence that the DNA molecules on the surface prepared by the backfilling method have the tendency to form aggregates. By contrast, the insertion method yields surfaces that are more uniform at the molecular scale. The presence of single-stranded segments in the thiolated DNA does not significantly reduce the quality of the monolayer surfaces during surface assembly, as MCH is sufficient to lift nonspecifically adsorbed probes off the gold. However, it remains difficult to controllably achieve the high probe density needed in practical sensors through insertion because the insertion process is limited by the intrinsic defects in the host SAM. Incorporation of novel probe structures[8, 24, 47] or direct covalent coupling of the probes atop a preformed, high-quality monolayer, rather than insertion of thiolated DNA or backfilling, may help to overcome these issues of SAM stability and probe aggregation. In addition, our study has also introduced spatial statistics that may allow us to connect the local environment of single molecules to relevant macroscopic properties. These molecular level insights may spur the development of new strategies to optimize molecular recognition or signaling reactions in DNA sensors.

## Materials and Methods

### Materials

Gold wire (99.99%, 1 mm diameter) was purchased from Scientific Instrument Services, Inc. 6-Mercapto-1-hexanol (MCH) was purchased from Santa Cruz Biotechnology, Inc. Tris-acetate-EDTA (TAE), 10× solution, and dithiothreitol (DTT), 99%, were purchased from Fisher Scientific. The synthetic oligonucleotides were purchased from IDT and used without further purification. Only ultrapure water (>18 MΩ·cm) generated from a Barnstead Diamond Nanopure water purification system was used.

### Preparation of the Thiolated DNA Probes

C6SH ds probes were prepared by PCR using M13mp18 RF I DNA (New England Biolabs) as the substrate and with primers C6SHF and C6SHR (full sequence of primers and complete probe in Supporting Information). The product was purified *via* agarose gel electrophoresis and Qiagen gel purification kit. Next, 50 μL of the purified PCR product was mixed with 15 μL of 1 M reducing agent DTT in Tris-EDTA buffer under nitrogen for >1 h, then washed using an illustra

NAP-5 column (GE Healthcare) and re-eluted in EDTA-supplemented 1× TAE solution (40 mM Tris-acetate, 10 mM EDTA) to a final concentration of ∼5–10 nM. DNA was stored in aliquots at −20 or −80 °C (long-term) until prior to assembly on the surface.

T5C6SH ss/ds probes were assembled by mixing 10 μL of 0.1 mM solutions of oligos T5C6SH1, T5C6SH2, T5C6SH3, and T5C6SH4 (sequences provided in Supporting Information) in 1× TAE. The mixture was heated in a thermocycler to 95 °C for 10 min, then cooled by 1 °C every 2 min until the temperature reached 20 °C, then held at 4 °C to stabilize. Structures were purified *via* agarose gel electrophoresis, and their thiol groups were reduced and the probes purified as above to a final concentration of ∼50 nM.

Surface Preparation and DNA Monolayer Preparation

A gold bead containing single-crystal Au(111) facets was made by melting a gold wire according to the method developed by Clavilier *et al.*[48] and then mounted on a platinum foil. This substrate was cleaned in hot nitric acid then annealed with a $H_2$ flame immediately prior to immersion in either "backfilling" (Figure 1C) or "insertion" (Figure 1D) method of assembly.

For backfilling method: A gold surface was exposed to 100× diluted solutions of either C6SH ds probe DNA or T5C6SH probes in EDTA-supplemented 1× TAE for lengths of time as described in the main text (10 s to 75 min), rinsed with 10× Tris-acetate-EDTA (400 mM Tris-acetate, 10 mM EDTA, TAE) buffer then immersed in a solution of 1:1 EtOH/$H_2O$ with 1× TAE containing a few drops of MCH (∼1–10 mM) for 60 min, then rinsed a second time with 1× TAE and imaged immediately afterward.

For insertion method: a solution of developed from 1:1 (by volume) 1× TAE in $H_2O$/ethanol containing 10–100 mM MCH. The bead was left overnight or up to a few days in the solution, rinsed with 1× TAE, and then immersed into a shallow beaker containing either C6SH or T5C6SH solutions for 3–10 min. The beads were rinsed copiously with 10× concentrated TAE solution (400 mM Tris-acetate, 10 mM EDTA), dried with a stream of filtered air, then loaded immediately into the AFM liquid cell.

Atomic Force Microscopy

An Agilent 5500 AFM was used for all experiments. *In situ* electrochemical AFM was performed under tapping mode in an aqueous 0.5× TAE solution (20 mM Tris-acetate, 0.5 mM EDTA) or sodium acetate (25 mM) supplemented with 1× TAE using a custom-built fluid cell containing a Pt/Ir wire (counter electrode) and a small Ag/AgCl reference electrode, which has a low leakage junction formed by the gap between a Pt wire and glass. SNL-10 (Bruker) probes with spring constants of approximately 0.2–0.4 N/m were used for all experiments. Occasionally, stiffer (5 N/m) AFM cantilevers were used at lower tapping amplitude to image T5C6SH probes at open circuit potential under liquid. The counter and reference electrodes as well as the fluid cell itself were cleaned in piranha solution (1:3 $H_2O_2$/$H_2SO_4$) prior to use and copiously rinsed with water. CAUTION: Piranha solution can react violently with organic materials and should be handled with personal protective equipment. Piranha solution should not be stored in tightly sealed containers. During imaging, topographical, amplitude, and phase channels were recorded

as well as potential applied from an integrated potentiostat in the AFM controller or from a BAS electrochemical workstation (Epsilon, Bioanalytical Systems). DNA topographical heights and locations were extracted using Gwyddion image analysis software and statistical analysis were performed using MATLAB.

## Supporting Information

Additional AFM images; complete sequence of oligonucleotides, primers and probes; details regarding the calculation of the crowding distribution function; and additional graphs of LCIs and n.n.d.s. This material is available at https://doi.org/10.1021/nn400659m.

## Acknowledgment

The authors acknowledge the support provided by UC Merced. E.A.J. was supported by the UC Merced Faculty Mentor Fellowship.

## References

1. Herne, T. M.; Tarlov, M. J. Characterization of DNA Probes Immobilized on Gold Surfaces J. Am. Chem. Soc. **1997**, 119, 8916– 8920 Google Scholar
2. Fan, C.; Plaxco, K. W.; Heeger, A. J. Electrochemical Interrogation of Conformational Changes as a Reagentless Method for the Sequence-Specific Detection of DNA Proc. Natl. Acad. Sci. U.S.A. **2003**, 100, 9134– 9137 Google Scholar
3. Drummond, T. G.; Hill, M. G.; Barton, J. K. Electrochemical DNA Sensors Nat. Biotechnol. **2003**, 21, 1192– 1199 Google Scholar
4. Peterson, A. W.; Heaton, R. J.; Georgiadis, R. M. The Effect of Surface Probe Density on DNA Hybridization Nucleic Acids Res. **2001**, 29, 5163– 5168 Google Scholar
5. Gong, P.; Levicky, R. DNA Surface Hybridization Regimes Proc. Natl. Acad. Sci. U.S.A. **2008**, 105, 5301– 5306 Google Scholar
6. Ricci, F.; Lai, R. Y.; Heeger, A. J.; Plaxco, K. W.; Sumner, J. J. Effect of Molecular Crowding on the Response of an Electrochemical DNA Sensor Langmuir **2007**, 23, 6827– 6834 Google Scholar
7. Wong, I. Y.; Melosh, N. A. Directed Hybridization and Melting of DNA Linkers using Counterion-Screened Electric Fields Nano Lett. **2009**, 9, 3521– 3526 Google Scholar
8. Pei, H.; Lu, N.; Wen, Y.; Song, S.; Liu, Y.; Yan, H.; Fan, C. A DNA Nanostructure-Based Biomolecular Probe Carrier Platform for Electrochemical Biosensing Adv. Mater. **2010**, 22, 4754– 4758 Google Scholar
9. Boman, F. C.; Gibbs-Davis, J. M.; Heckman, L. M.; Stepp, B. R.; Nguyen, S. T.; Geiger, F. M. DNA at Aqueous/Solid Interfaces: Chirality-Based Detection *via* Second Harmonic Generation Activity J. Am. Chem. Soc. **2008**, 131, 844– 848 Google Scholar

10. Caruso, F.; Rodda, E.; Furlong, D. N.; Niikura, K.; Okahata, Y. Quartz Crystal Microbalance Study of DNA Immobilization and Hybridization for Nucleic Acid Sensor Development Anal. Chem. **1997**, 69, 2043– 2049 Google Scholar

11. Steel, A. B.; Herne, T. M.; Tarlov, M. J. Electrochemical Quantitation of DNA Immobilized on Gold Anal. Chem. **1998**, 70, 4670– 4677 Google Scholar

12. Josephs, E. A.; Ye, T. A Single-Molecule View of Conformational Switching of DNA Tethered to a Gold Electrode J. Am. Chem. Soc. **2012**, 134, 10021– 10030 Google Scholar

13. Josephs, E. A.; Ye, T. Electric-Field Dependent Conformations of Single DNA Molecules on a Model Biosensor Surface Nano Lett. **2012**, 12, 5255– 5261 Google Scholar

14. Wernette, D. P.; Mead, C.; Bohn, P. W.; Lu, Y. Surface Immobilization of Catalytic Beacons Based on Ratiometric Fluorescent DNAzyme Sensors: A Systematic Study Langmuir **2007**, 23, 9513– 9521 Google Scholar

15. Yao, G.; Tan, W. Molecular-Beacon-Based Array for Sensitive DNA Analysis Anal. Biochem. **2004**, 331, 216– 223 Google Scholar

16. Pavlov, V.; Xiao, Y.; Gill, R.; Dishon, A.; Kotler, M.; Willner, I. Amplified Chemiluminescence Surface Detection of DNA and Telomerase Activity Using Catalytic Nucleic Acid Labels Anal. Chem. **2004**, 76, 2152– 2156 Google Scholar

17. White, R. J.; Rowe, A. A.; Plaxco, K. W. Re-engineering Aptamers To Support Reagentless, Self-Reporting Electrochemical Sensors Analyst **2010**, 135, 589– 594 Google Scholar

18. Hurst, S. J.; Lytton-Jean, A. K. R.; Mirkin, C. A. Maximizing DNA Loading on a Range of Gold Nanoparticle Sizes Anal. Chem. **2006**, 78, 8313– 8318 Google Scholar

19. Hansma, H. G. Surface Biology of DNA by Atomic Force Microscopy Annu. Rev. Phys. Chem. **2001**, 52, 71– 92 Google Scholar

20. Rant, U.; Pringsheim, E.; Kaiser, W.; Arinaga, K.; Knezevic, J.; Tornow, M.; Fujita, S.; Yokoyama, N.; Abstreiter, G. Detection and Size Analysis of Proteins with Switchable DNA Layers Nano Lett. **2009**, 9, 1290– 1295 Google Scholar

21. Rant, U.; Arinaga, K.; Scherer, S.; Pringsheim, E.; Fujita, S.; Yokoyama, N.; Tornow, M.; Abstreiter, G. Switchable DNA Interfaces for the Highly Sensitive Detection of Label-Free DNA Targets Proc. Natl. Acad. Sci. U.S.A. **2007**, 104, 17364– 17369 Google Scholar

22. Rant, U.; Arinaga, K.; Fujita, S.; Yokoyama, N.; Abstreiter, G.; Tornow, M. Electrical Manipulation of Oligonucleotides Grafted to Charged Surfaces Org. Biomol. Chem. **2006**, 4, 3448– 3455 Google Scholar

23. Willner, I.; Zayats, M. Electronic Aptamer-Based Sensors Angew. Chem., Int. Ed. **2007**, 46, 6408– 6418 Google Scholar

24. Lubin, A. A.; Vander Stoep Hunt, B.; White, R. J.; Plaxco, K. W. Effects of Probe Length, Probe Geometry, and Redox-Tag Placement on the Performance of the Electrochemical E-DNA Sensor Anal. Chem. **2009**, 81, 2150– 2158 Google Scholar

25. Swearingen, C. B.; Wernette, D. P.; Cropek, D. M.; Lu, Y.; Sweedler, J. V.; Bohn, P. W. Immobilization of a Catalytic DNA Molecular Beacon on Au for Pb(II) Detection Anal. Chem. **2005**, 77, 442– 448 Google Scholar

26. Schreiner, S. M.; Hatch, A. L.; Shudy, D. F.; Howard, D. R.; Howell, C.; Zhao, J.; Koelsch, P.; Zharnikov, M.; Petrovykh, D. Y.; Opdahl, A. Impact of DNA-Surface Interactions on the Stability of DNA Hybrids Anal. Chem. **2011**, 83, 4288– 4295 Google Scholar

27. Chen, Y.; Wang, M. S.; Mao, C. D. An Autonomous DNA Nanomotor Powered by a DNA Enzyme Angew. Chem., Int. Ed. **2004**, 43, 3554– 3557 Google Scholar

28. Chen, Y.; Mao, C. Putting a Brake on an Autonomous DNA Nanomotor J. Am. Chem. Soc. **2004**, 126, 8626– 8627 Google Scholar

29. Arinaga, K.; Rant, U.; Knezevic, J.; Pringsheim, E.; Tornow, M.; Fujita, S.; Abstreiter, G.; Yokoyama, N. Controlling the Surface Density of DNA on Gold by Electrically Induced Desorption Biosens. Bioelectron. **2007**, 23, 326– 331 Google Scholar

30. Murphy, J. N.; Cheng, A. K. H.; Yu, H. Z.; Bizzotto, D. On the Nature of DNA Self-Assembled Monolayers on Au: Measuring Surface Heterogeneity with Electrochemical *In Situ* Fluorescence Microscopy J. Am. Chem. Soc. **2009**, 131, 4042– 4050 Google Scholar

31. Barton, J. K.; Kelley, S. O.; Jackson, N. M.; McPherson, L. D.; Potter, A. B.; Spain, E. M.; Allen, M. J.; Hill, M. G. Orienting DNA Helices on Gold Using Applied Electric Fields Langmuir **1998**, 14, 6781– 6784 Google Scholar

32. Sam, M.; Boon, E. M.; Barton, J. K.; Hill, M. G.; Eileen, M. Morphology of 15-Mer Duplexes Tethered to Au(111) Probed Using Scanning Probe Microscopy Langmuir **2001**, 17, 5727– 5730 Google Scholar

33. Liu, M.; Liu, G. Y. Hybridization with Nanostructures of Single-Stranded DNA Langmuir **2005**, 21, 1972– 1978 Google Scholar

34. Mirmomtaz, E.; Castronovo, M.; Grunwald, C.; Bano, F.; Scaini, D.; Ensafi, A. A.; Scoles, G.; Casalis, L. Quantitative Study of the Effect of Coverage on the Hybridization Efficiency of Surface-Bound DNA Nanostructures Nano Lett. **2008**, 8, 4134– 4139 Google Scholar

35. Bosco, A.; Bano, F.; Parisse, P.; Casalis, L.; DeSimone, A.; Micheletti, C. Hybridization in Nanostructured DNA Monolayers Probed by AFM: Theory *versus* Experiment Nanoscale **2012**, 4, 1734– 1741 Google Scholar

36. Yamada, R.; Uosaki, K. *In Situ* Scanning Tunneling Microscopy Observation of the Self-Assembly Process of Alkanethiols on Gold (111) in Solution Langmuir **1998**, 14, 855– 861 Google Scholar

37. Keighley, S. D.; Li, P.; Estrela, P.; Migliorato, P. Optimization of DNA Immobilization on Gold Electrodes for Label-Free Detection by Electrochemical Impedance Spectroscopy Biosens. Bioelectron. **2008**, 23, 1291– 1297 Google Scholar

38. Poirier, G. E.; Pylant, E. D.; White, J. M. Crystalline Structures of Pristine and Hydrated Mercaptohexanol Self-Assembled Monolayers on Au(111) J. Chem. Phys. **1996**, 105, 2089– 2092 Google Scholar

39. Shuster, M. J.; Vaish, A.; Szapacs, M. E.; Anderson, M. E.; Weiss, P. S.; Andrews, A. M. Biospecific Recognition of Tethered Small Molecules Diluted in Self-Assembled Monolayers Adv. Mater. **2008**, 20, 164 Google Scholar

40. Bumm, L. A.; Arnold, J. J.; Cygan, M. T.; Dunbar, T. D.; Burgin, T. P.; Jones, L.; Allara, D. L.; Tour, J. M.; Weiss, P. S. Are Single Molecular Wires Conducting? Science **1996**, 271, 1705– 1707 Google Scholar

41. Heaton, R. J.; Peterson, A. W.; Georgiadis, R. M. Electrostatic Surface Plasmon Resonance: Direct Electric Field-Induced Hybridization and Denaturation in Monolayer Nucleic Acid Films and Label-Free Discrimination of Base Mismatches Proc. Natl. Acad. Sci. U.S.A. **2001**, 98, 3701– 3704 Google Scholar

42. White, R. J.; Phares, N.; Lubin, A. A.; Xiao, Y.; Plaxco, K. W. Optimization of Electrochemical Aptamer-Based Sensors *via* Optimization of Probe Packing Density and Surface Chemistry Langmuir **2008**, 24, 10513– 10518 Google Scholar

43. Wong, I. Y.; Melosh, N. A. An Electrostatic Model for DNA Surface Hybridization Biophys. J. **2010**, 98, 2954– 2963 Google Scholar

44. Diggle, P. In Statistical Analysis of Spatial Point Patterns; Oxford University Press: London, 2003. Google Scholar

45. Getis, A.; Franklin, J. Second-Order Neighborhood Analysis of Mapped Point Patterns Ecology **1987**, 473– 477 Google Scholar

46. Ripley, B. D. The Second-Order Analysis of Stationary Point Processes J. Appl. Prob. **1976**, 255– 266 Google Scholar

47. Wen, Y.; Pei, H.; Shen, Y.; Xi, J.; Lin, M.; Lu, N.; Shen, X.; Li, J.; Fan, C. DNA Nanostructure-Based Interfacial Engineering for PCR-Free Ultrasensitive Electrochemical Analysis of microRNA Sci. Rep. **2012**, 2, 867 Google Scholar

48. Clavilier, J.; Faure, R.; Guinet, G.; Durand, R. Preparation of Mono-crystalline Pt Microelectrodes and Electrochemical Study of the Plane Surfaces Cut in the Direction of the (111) and (110) Planes J. Electroanal. Chem. **1980**, 107, 205– 209 Google Scholar